First-principles calculations of effective-mass parameters of AlN and GaN

Masakatsu Suzuki and Takeshi Uenoyama
Central Research Laboratories, Matsushita Electric Industrial Co., Ltd., Hikaridai, Seikacho, Kyoto 619-02, Japan

Akira Yanase
College of Integrated Arts and Science, University of Osaka Prefecture, Sakai, Osaka 591, Japan
(Received 8 March 1995; revised manuscript received 15 May 1995)

The electronic band structures of the wurtzite-type AlN and GaN are calculated by using a self-consistent full-potential linearized augmented plane-wave method within the local-density-functional approximation. In order to clarify the electronic properties near the Brillouin-zone (BZ) center and to give an important guideline on the material designs for short-wavelength optical devices, we link the first-principles band calculations with the effective-mass approximation. The electronic properties are analytically studied on the basis of the effective-mass Hamiltonian, where we consider the hexagonal symmetry of the wurtzite structure. The effective-mass parameters, such as electron effective mass, hole effective masses, or, equivalently, the Luttinger-like parameters, crystal-field splitting and spin-orbit splitting, are determined by reproducing the calculated band structures near the BZ center. The obtained results show that the cubic approximation is fairly successful in the analysis for the valence-band structures of the wurtzite-type nitrides. Further, the calculated parameters for GaN are consistent with the observed ones.

I. INTRODUCTION

The group-III nitrides AIN, GaN, and InN usually crystallize in the wurtzite (WR)-type crystal structure. These materials have attracted much attention as candidates for optical devices in visible and ultraviolet (UV) regions, since they have direct transition-type band structures with band gaps widely ranging from 1.9 eV for InN (Ref. 1) through 3.4 eV for GaN (Ref. 2) to 6.2 eV for AIN (Ref. 3) at room temperature. In particular most of the recent interest has focused on the fabrication of short-wavelength devices, such as light-emitting diodes (LED's), and laser diodes (LD's) in blue and/or UV regions.

However, technological applications have never been achieved owing to two significant problems. One is that there are no suitable substrate materials with a close lattice match. Although a sapphire (0001) is used for the substrate in most experiments, three-dimensional (3D) growth is unavoidable due to the lattice mismatch. The other is that *n*-type conduction, with electron concentrations of $10^{18}-10^{19}$ cm^{-3}, makes it difficult to grow the *p*-type crystals. The origin of such high electron concentrations is usually assumed to be N vacancies due to a lack of residual impurities. Thus much effort has been made for a long time to grow high-quality materials.

In recent years, these difficulties were considerably overcome by a two-step growth technique, which uses a preceding growth of thin AlN (Ref. 4) or GaN (Ref. 5) at low temperature as buffer layers. This approach effectively suppresses the 3D growth of these nitrides on the sapphire substrate, and the crystallographic, electrical, and optical properties are remarkably improved. Furthermore, as for the *p*-type doping, it was found that hole carrier concentrations are improved by low-energy electron-beam irradiation (LEEBI),[6] or by a thermal annealing in a N_2 gas atmosphere[7] of Mg-doped crystals. As a result of these treatments, efficient bright blue LED's using a $In_xGa_{1-x}N/Al_xGa_{1-x}N$ double heterostructure (DH) have been fabricated, and experimental efforts have been directed to realizing blue LD's.

In theoretical studies, several band-structure calculations have been published for AlN and GaN with some crystal structures.[8-15] Most of their results show the density of states, charge-density distributions, and structural properties such as the bulk modulus and pressure dependence of the band gap. In spite of these calculations, electronic properties such as effective masses and energy splittings have scarcely been investigated even for the WR structure. On the other hand, experimental data are also scarce due to the above difficulties. Therefore, it is very important to determine the above electronic parameters, which are indispensable for material and device designs based on the quantum theory.

The purpose of this study is to clarify the electronic properties of the WR-type AlN and GaN, and to give an important guideline on the material designs of short-wavelength optical devices using these nitrides. Therefore, we focus on electronic structures around the valence-band maximum (VBM) and the conduction-band minimum (CBM), and link the electronic band calculation with the effective-mass theory. At first, first-principles electronic band calculations of WR-type AlN and GaN are performed. Then we analytically investigate the electronic properties on the basis of the effective-mass Hamiltonian, where we consider the hexagonal symmetry of the WR structure. Effective-mass parameters such as electron effective mass, hole effective masses, or, equivalently, Luttinger-like parameters, crystal-field splitting and spin-orbit splitting, are derived

0163-1829/95/52(11)/8132(8)/$06.00

from reproducing the calculated band structures around the VBM and CBM. As a result, we present significant parameters of these materials, which can be used for the design of optical devices like LD's.

This paper is organized as follows. In Sec. II, the method and results of the first-principles calculations are described. In Sec. III, we explain the effective-mass approximation for the WR structure. In Sec. IV, numerical results for the electronic properties are presented. Section V summarizes the present studies.

II. ELECTRONIC BAND STRUCTURE

A. Method of FLAPW calculations

AlN and GaN usually have WR structure (space group C_{6v}^4) and zinc-blende (ZB) structure (space group T_d^2) as well. In this study, in order to understand the electronic properties of AlN and GaN in the WR structure, electronic band calculations have been performed by using a full-potential linearized augmented plane-wave (FLAPW) method.[16] The local-density approximation (LDA) is used to construct exchange-correlation terms of the one-electron potential.[17] The spin-orbit interaction is considered as a perturbation to the scalar-relativistic Hamiltonian. The $3d$ electrons of the Ga atom are treated as part of the valence-band states, since they are relatively high in energy even though they constitute a well-localized narrow band.

Inside the muffin-tin (MT) spheres, the angular momentum expansion is truncated at $l_{\max}=7$ for the wave functions. A set of LAPW basis functions is constructed within the criterion that $|\mathbf{k}+\mathbf{G}|_{\max}=5.5(2\pi/a)$, with $\mathbf{k}$ being a wave vector in the first Brillouin zone (BZ) shown in Fig. 1, and $\mathbf{G}$ being a reciprocal-lattice vector. This criterion yields a set of about 390 LAPW basis functions. The charge density has been self-consistently determined using 28 meshed $\mathbf{k}$ points in an irreducible wedge of the first BZ. The iteration process has been repeated until the calculated total energy of the crystal converges into less than 1 mRy.

The lattice parameters used in the present calculations are $a=5.8808$ a.u., $c=9.4146$ a.u. for AlN, and $a=6.0263$ a.u., $c=9.7982$ a.u. for GaN. These values are the experimental ones.[2,3] The internal parameter u, which is the relative displacement of the N sublattice with respect to the Al or Ga sublattice along the c direction, was fixed at the ideal value of $0.375c$. The MT sphere radii for Al, Ga, and N were the same values of $0.21a$, since the use of the full potential ensures that the calculation is completely independent of the choice of MT sphere radii.

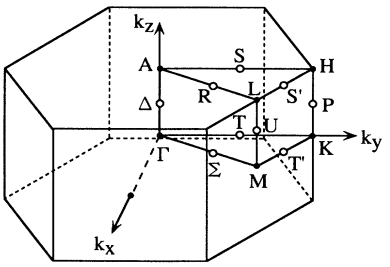

FIG. 1. The first Brillouin zone for the wurtzite-type crystals.

B. Results of FLAPW calculations

The calculated band structures for the WR-type AlN and GaN are in good agreement with previous theoretical results using the LDA.[8,11,13,14] It is well known that the LDA yields quite reliable ground-state properties, but seriously underestimates the band gap for all usual semiconductors. A more accurate band structure is achieved by the quasiparticle approach using the GW approximation.[18–20] The GW calculation was applied to these materials as well.[14,15] The results show that there is a $\mathbf{k}$-directional dependence on the quasiparticle correction for AlN and GaN. However, in general, the LDA wave functions are very close to the corrected ones, and the correction causes a rigid shift of the conduction band against the valence band and, at the same time, broadening of both bands. Now we are mainly interested in the band structure in close proximity to the VBM and the CBM, which are the Γ points for the WR-type AlN and GaN. Therefore, the $\mathbf{k}$-directional dependence on the GW correction is negligible, and the LDA calculation seems to be sufficiently accurate for our purposes.

In this paper, as an example, the characteristics of the result for GaN are described, compared with the previous calculations. We show the electronic band structure of GaN by the FLAPW band calculation without the spin-orbit interaction in Fig. 2, where the energy dispersions along high-symmetry lines of the first BZ (see Fig. 1) are shown. The energy bands consist of four parts, three occupied bands and an unoccupied band.

The lowest-energy bands, which are localized between about -0.7 and -0.65 Ry, mostly originate from N $2s$ states. The upper side of these states are hybridized with Ga $3d$ states. The second-lowest-energy bands are locat-

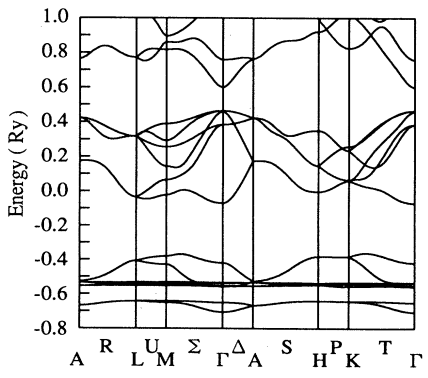

FIG. 2. The electronic band structure of the WR type GaN without spin-orbit interaction. The energy dispersions along the high-symmetry lines in the first BZ (see Fig. 1) are shown.

ed between about −0.55 and −0.38 Ry, where the lower-energy side almost originates from Ga 3*d* well-localized states, and the upper one consists of the hybridized states between Ga 3*d* and N 2*s* states. Due to these hybridizations, Ga 3*d* states must be included in the valence-band states, as mentioned above and pointed out in Refs. 12 and 13. In the case of AlN, there is no hybridization between cation *d* and N 2*s* states, since the Al atom has no *d* electrons. Consequently, the lowest-energy band is combined with the upper side of the second-lowest one, and these two bands become one narrow band.

In the intermediate-energy region, there are broad energy bands whose width is about 0.53 Ry. The VBM is the top of these bands, and is located at the Γ point. These energy bands arise from N 2*s*, 2*p* and Ga 4*s*, 4*p* states; however, the vicinity of the VBM consists almost exclusively of N 2*p* states. The highest-energy region, which is higher than about 0.6 Ry, is the conduction band, and the CBM is located at the Γ point as well. The vicinity of the CBM originates from N and Ga *s* states. Our result for the characters around the VBM and CBM is consistent with that of the previous study.[12] Comparing the results of AlN and GaN, the main features in these two energy regions are very similar, except for the order of energy levels around the VBM.

Here our attention is directed to the vicinity of the VBM. We note that the band structures around the VBM are different from the ZB-type crystal. Figure 3 shows schematic band structures near the Γ point without and with the spin-orbit interaction. Even in the absence of the spin-orbit interaction, the top of the valence band is split into twofold- and single-degenerate states. Using irreducible representations of group theory, the former state is labeled Γ_6, whose wave functions transform like *x* and *y*, and the latter one is labeled Γ_1 whose wave function transforms like *z*. The energy splitting between these two levels is induced by the hexagonal symmetry of the WR structure, therefore this splitting is called the crystal-field splitting Δ_{cr}. The order of the two levels depends on the kind of materials and the ratio c/a of lattice constants. In the case of GaN, the Γ_6 level is higher than the Γ_1 level, while in the case of AlN the Γ_1 level is higher. This difference between AlN and GaN is in agreement with the result in Ref. 14.

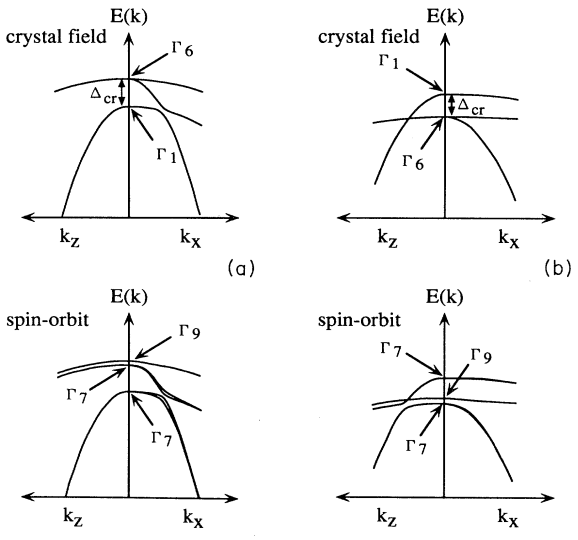

FIG. 3. Schematic band structures near the Γ point of (a) GaN and (b) AlN without and with spin-orbit interaction.

Introducing the spin-orbit interaction, the twofold degenerate Γ_6 level is split into Γ_9 and Γ_7 levels. Then the single-degenerate Γ_1 level is labeled Γ_7 as well, and the two Γ_7 levels are mixed. The energy splittings among these three levels by the spin-orbit coupling is called a spin-orbit splitting. According to our calculations, spin-orbit splittings are much smaller than the crystal-field splitting in these nitrides, though the crystal-field splitting itself is small. The values of the energy splittings are discussed in Sec. IV.

III. EFFECTIVE-MASS APPROXIMATION

In general, transport and optical phenomena usually involve the information of only a small region of **k** space. In other words, the above characteristics of these systems are governed by the band structures in the immediate vicinity of the BZ center. Thus the effective-mass approximation is an appropriate method to make an analysis of the electronic properties tractable. In this section, we explain the effective-mass approximation for the conduction and valence bands of the WR structure, and discuss the electronic properties near the BZ center.

A. Formulation

In ZB-type crystals, a parabolic band is assumed for the electronic structure around the CBM, and the Luttinger-Kohn Hamiltonian is used to describe that around the VBM.[21] According to our calculations, the lowest conduction band consists almost exclusively of Ga (Al) and N *s* states, which is also the case in ZB-type crystals, and the *s*-like conduction band is isotropic in contrast to the valence band, which shows a strong anisotropy. Therefore, if a small anisotropy of energy dispersions is neglected, (i.e., if the parabolic band is assumed), the electronic structure around the CBM is given by the following relation:

$$E_c(\mathbf{k}) = E_g + \mathbf{k}^2/2m_c^* , \tag{1}$$

where m_c^* denotes the electron effective mass around the CBM.

On the other hand, the Luttinger-Kohn Hamiltonian cannot describe the valence-band structure of the WR-type crystals, since it reflects the cubic symmetry of the ZB structure. Thus we must consider the hexagonal symmetry of the WR structure. In general, the effective-mass Hamiltonian is derived from either an invariant theory or a perturbation theory. In this study, we use the former one and expand the Hamiltonian within the second order of **k**. Then we can obtain the effective-mass Hamiltonian for the WR structure as follows:[22]

$$\mathcal{H}(\mathbf{k})=\Delta_1 L_z^2+\Delta_2 L_z\sigma_z+\sqrt{2}\Delta_3(L_+\sigma_-+L_-\sigma_+)+(A_1+A_3L_z^2)k_z^2+(A_2+A_4L_x^2)(k_x^2+k_y^2)$$
$$-A_5(L_+^2k_-^2+L_-^2k_+^2)-2iA_6k_z([L_z,L_+]k_--[L_z,L_-]k_+)+A_7(k_-L_++k_+L_-)\ , \tag{2}$$

where $\mathbf{L}$ and σ denote the orbital and spin angular momentum operators, respectively, and $\mathbf{k}$ represents the wave vector in the first BZ. $L_\pm$, $\sigma_\pm$, and $k_\pm$ are defined by

$$L_\pm\equiv\pm(i/\sqrt{2})(L_x\pm iL_y)\ ,$$
$$\sigma_\pm\equiv\pm(i/2)(\sigma_x\pm i\sigma_y)\ , \tag{3}$$
$$k_\pm\equiv k_x\pm ik_y\ ,$$

and atomic units (i.e., $\hbar=1$, $m_0=\frac{1}{2}$, and $e^2=2$) and energies in Ry are used in this study.

Here $A_i(i=1-7)$ represents the parameters corresponding to hole effective masses, or equivalently, the Luttinger parameters, and $\Delta_i(i=1-3)$ denotes the parameters characterizing energy splittings at $\mathbf{k}=\mathbf{0}$. Δ_1 corresponds to the energy splitting induced by the hexagonal symmetry, and Δ_2 and Δ_3 correspond to those by the spin-orbit interaction. Here there seems to be little contribution of the $\mathbf{k}$ linear relativistic effect in these materials, since the upper part of the valence band almost arises from N $2p$ states according to first-principles calculations. Generally, the relativistic effects on N $2p$ states are not so much. Thus we consider the spin-orbit interaction only at $\mathbf{k}=\mathbf{0}$ and neglect the $\mathbf{k}$ linear relativistic terms.

Next, in order to obtain the matrix representation of this Hamiltonian, we adopt the following functions as the basis functions, which make L_z and σ_z diagonalized:

$$(1/\sqrt{2})|(X+iY),\alpha\rangle,\quad (1/\sqrt{2})|(X+iY),\beta\rangle\ ,$$
$$|Z,\alpha\rangle,\quad |Z,\beta\rangle\ ,$$
$$(1/\sqrt{2})|(X-iY),\alpha\rangle,\quad (1/\sqrt{2})|(X-iY),\beta\rangle\ ,$$

where $|X\rangle$, $|Y\rangle$, and $|Z\rangle$ are Bloch functions at the Γ point, transforming like x, y, and z, respectively, and $|\alpha\rangle$ and $|\beta\rangle$ are spin functions corresponding to spin-up and -down, respectively. Using the above six basis functions, the Hamiltonian is explicitly expressed as

$$\mathbf{H}(\mathbf{k})=\begin{bmatrix} F & 0 & -H^* & 0 & K^* & 0 \\ 0 & G & \Delta & -H^* & 0 & K^* \\ -H & \Delta & \lambda & 0 & I^* & 0 \\ 0 & -H & 0 & \lambda & \Delta & I^* \\ K & 0 & I & \Delta & G & 0 \\ 0 & K & 0 & I & 0 & F \end{bmatrix}, \tag{4}$$

where F, G, H, I, K, Δ, λ, and θ are defined by

$$F=\Delta_1+\Delta_2+\lambda+\theta\ ,$$
$$G=\Delta_1-\Delta_2+\lambda+\theta\ ,$$
$$H=iA_6k_zk_+-A_7k_+\ ,$$
$$I=iA_6k_zk_++A_7k_+\ ,$$
$$K=A_5k_+^2\ , \tag{5}$$
$$\Delta=\sqrt{2}\Delta_3\ ,$$
$$\lambda=A_1k_z^2+A_2(k_x^2+k_y^2)\ ,$$
$$\theta=A_3k_z^2+A_4(k_x^2+k_y^2)\ .$$

Here we discuss the relations among the above parameters from the point of view of the local symmetry. Note that the local coordination on the atomic position of the WR structure is the same as that of the ZB structure. The two structures are different mainly at the relative positions of the third neighbors and beyond. In both types of crystals, one kind of atom is tetrahedrally surrounded by the other kind of atom. The layer stacking of the WR crystal along the (0001) direction corresponds to that of the ZB crystal along the (111) direction. Thus we introduce the following approximation, which is called the cubic approximation.[22] At first, let us transform the Luttinger-Kohn Hamiltonian for the ZB structure to another coordinate system, in which the z' axis is along the (111) direction and the x' and y' axes along the $(11\bar{2})$ and $(\bar{1}10)$ directions, respectively. Next, comparing this transformed Hamiltonian with the above Hamiltonian for the WR structure, we can establish the relations among the parameters A_is and Δ_is. They are satisfied with the following relations:

$$A_1=A_2+2A_4\ ,$$
$$A_3=-2A_4\ ,$$
$$A_3+4A_5=\sqrt{2}A_6\ , \tag{6}$$
$$A_7=0\ ,$$
$$\Delta_2=\Delta_3\ .$$

According to these equations, independent parameters are three A_i and two Δ_i. Therefore, we must determine at least five parameters, for example A_1, A_3, A_5, Δ_1, and Δ_2, to reproduce the band structures near the VBM. Then the energy levels $E(\mathbf{k})$ on the effective-mass approximation can be obtained by solving the following equation:

$$D(\mathbf{k})=\det|\mathbf{H}(\mathbf{k})-E(\mathbf{k})\mathbf{I}|=0\ , \tag{7}$$

where $\mathbf{I}$ is a 6×6 unit matrix.

B. Analytical solutions

First we show the analytical solutions of the effective-mass Hamiltonian at the Γ point. The Hamiltonian gives the energy levels at $\mathbf{k}=\mathbf{0}$ as follows:

$$E_1^0=\Delta_1+\Delta_2\ ,$$
$$E_{2,3}^0=\frac{\Delta_1-\Delta_2\pm\sqrt{(\Delta_1-\Delta_2)^2+8\Delta_3^2}}{2}\ , \tag{8}$$

where E_1^0 corresponds to the Γ_9 level and $E_{2,3}^0$ corresponds to the two Γ_7 levels. As for the double sign, the plus sign corresponds to E_2^0 and the minus sign to E_3^0. According to these equations, in the absence of the spin-orbit coupling ($\Delta_2=\Delta_3=0$), $E_1^0=E_2^0$, $E_{1,2}^0-E_3^0=\Delta_1$ for $\Delta_1>0$, and $E_1^0=E_3^0$, $E_{1,3}^0-E_2^0=\Delta_1$ for $\Delta_1<0$. Thus Δ_1 is called the crystal-field splitting Δ_{cr}. On the other hand, considering no hexagonal crystal field ($\Delta_1=0, \Delta_2=\Delta_3$), $E_1^0=E_2^0$, $E_{1,2}^0-E_3^0=3\Delta_2$ for $\Delta_{2,3}>0$, and $E_1^0=E_3^0$, $E_{1,3}^0-E_2^0=3\Delta_2$ for $\Delta_{2,3}<0$. Then, the quantity $3\Delta_2(=3\Delta_3)$ corresponds to the spin-orbit splitting Δ_{so} in the ZB-type crystals.

Next we study the analytical expressions for energy eigenvalues at general $\mathbf{k}$ points. Assuming that $\Delta_2=\Delta_3=0$ ($F=G, \Delta=0$), or neglecting the spin-orbit coupling, the Hamiltonian is easily diagonalized, and the energy dispersions are given as follows:

$$E_1=F'-K'\ ,$$
$$E_{2,3}=\frac{F'+K'+\lambda\pm\sqrt{(F'+K'-\lambda)^2+8H'^2}}{2}\ , \tag{9}$$

where F', K', and H' are defined by

$$F'=\Delta_1+(A_1+A_3)k_z^2+(A_2+A_4)(k_x^2+k_y^2)\ ,$$
$$K'=A_5(k_x^2+k_y^2)\ , \tag{10}$$
$$H'=\sqrt{(A_6^2k_z^2+A_7^2)(k_x^2+k_y^2)}\ .$$

As for the double sign, the plus sign corresponds to E_2 and the minus sign to E_3. According to these equations, the energy dispersions of E_i are isotropic in the k_x-k_y plane within the second-order expansion of $\mathbf{k}$. In case of $\Delta_1>0$ ($\Delta_1<0$), the effective masses of three energy bands, $E_{1(1)}$, $E_{2(3)}$, and $E_{3(2)}$ at $\mathbf{k}=\mathbf{0}$ correspond to heavy-, light- and split-off-hole masses, respectively. Each hole mass can be obtained from the second derivative of the above analytical expressions. Thus the hole masses along the k_z direction ($m^{\parallel}$) and those in the k_x-k_y plane ($m^{\perp}$) are given as follows.

k_z direction ($k_z=k_y=0$):

$$m_0/m^{\parallel}_{hh}=-(A_1+A_3)\ ,$$
$$m_0/m^{\parallel}_{lh}=-(A_1+A_3)\ , \tag{11}$$
$$m_0/m^{\parallel}_{split}=-A_1\ .$$

k_x-k_y plane ($k_z=0$):

$$m_0/m^{\perp}_{hh}=-(A_2+A_4-A_5)\ ,$$
$$m_0/m^{\perp}_{lh}=-(A_2+A_4+A_5)-2A_7^2/|\Delta_1|\ , \tag{12}$$
$$m_0/m^{\perp}_{split}=-A_2+2A_7^2/|\Delta_1|\ ,$$

where the subscripts, hh, lh, and split denote the heavy-, light-, and split-off-hole bands, respectively. The naming of three hole bands is based on the feature in the k_x-k_y plane. The features are discussed in Sec. IV.

IV. NUMERICAL RESULTS

A. Effective-mass parameters

Now we know the energy levels for arbitrary $\mathbf{k}$ points thanks to the first-principles calculations, but the effective-mass parameters m_c^* for the conduction band, and A_i and Δ_i for the valence band, are almost unknown. Thus we investigated the finer electronic band structures near the Γ point by using the energy eigenvalues at three-dimensional (3D) dense meshed $\mathbf{k}$ points from first-principles calculations. Then we derived the above parameters by reproducing the band structures near the Γ point on the basis of the effective-mass Hamiltonian.

First we show the calculated results of the electron effective mass. According to our first-principles calculations, the energy dispersion of the lowest conduction band has some anisotropy for $\mathbf{k}$ directions. Therefore, the electron effective mass was determined by averaging the $\mathbf{k}$-direction-dependent masses over a number of directions. Each $\mathbf{k}$-direction-dependent one is obtained by fitting the energy dispersion of the lowest conduction band to a parabolic function in the vicinity of the Γ point. The calculated electron effective masses for AlN and GaN are summarized in Table I, where m_c^*, $m_c^{\parallel}$, and $m_c^{\perp}$ denote the average electron effective mass and the $\mathbf{k}$-direction-dependent ones along k_z and k_x directions, respectively. The obtained value for GaN is in good agreement with the observed values, $0.22m_0$ and $0.20m_0$.[23,24]

Next we show the numerical results of the valence-band parameters A_i and Δ_i. Here, it is very difficult to accurately determine the ten parameters at the same time. Thus we adopted the cubic approximation for simplicity, and performed the least-square fitting of the energy levels at 3D meshed $\mathbf{k}$ points in the vicinity of the Γ point. This procedure is called 3D fitting. In this procedure, we minimized the function, $\sum_i |D(\mathbf{k}_i)|^2$, where $\mathbf{k}_i$s are meshed sampling $\mathbf{k}$ points. The calculated results for AlN and GaN are summarized in Table II. Further, we show the upper valence-band structure of GaN in Fig. 4, where two kinds of results are shown together. The broken lines are the result by diagonalizing the 6×6 effective-mass Hamiltonian using the obtained parame-

TABLE I. The electron effective masses for AlN and GaN. m_c^*, $m_c^{\parallel}$, and $m_c^{\perp}$ denote the average electron effective mass and the $\mathbf{k}$-direction-dependent masses along the k_z and k_x directions, respectively. All values are in units of a free-electron mass m_0.

	m_c^*	$m_c^{\parallel}$	$m_c^{\perp}$
AlN	0.27	0.33	0.25
GaN	0.18	0.20	0.18

TABLE II. The valence-band parameters A_i and Δ_i for AlN and GaN. A_i ($i=1-6$) denotes the hole effective masses, or equivalently the Luttinger-like parameters, in units of $\hbar^2/2m_0$. Δ_i ($i=1-3$) represents the energy splittings at the Γ point in units of mRy. The results of the line fitting for A_is (except A_6) and the Γ-point fitting for Δ_is are also listed in round brackets, compared with that of the 3D fitting within the cubic approximation.

	A_1	A_2	A_3	A_4	A_5	A_6	Δ_1	Δ_2	Δ_3
AlN	−3.95	−0.27	3.68	−1.84	−1.95	−2.91	−4.30	0.50	0.50
	(−4.06)	(−0.26)	(3.78)	(−1.86)	(−2.02)	(-)	(−4.3)	(0.5)	(0.5)
GaN	−6.56	−0.91	5.65	−2.83	−3.13	−4.86	5.36	0.38	0.38
	(−6.27)	(−0.96)	(5.70)	(−2.84)	(−3.18)	(-)	(5.3)	(0.4)	(0.5)

ters, and the open circles are the result by the FLAPW band calculation with the spin-orbit interaction. From the comparison between two results, it is found that the 3D fitting within the cubic approximation is in good agreement with the FLAPW calculation.

Since A_i are merely fitting parameters which are physically meaningless, we discuss the feature of three hole bands around the VBM. The hole effective masses are obtained by using values of A_i. The calculated hole masses for AlN and GaN are summarized in Table III, where $m_{\rm hh}$, $m_{\rm lh}$, and $m_{\rm split}$ correspond to Γ_9^6 (heavy), Γ_7^6 (light), and Γ_7^1 (split-off) bands, respectively. The subscripts and superscripts stand for the labels of irreducible representation in the case with and without the spin-orbit coupling, respectively. The naming of three hole bands, heavy, light, and split-off, is based on the feature in the k_x-k_y plane. According to our calculations, the hole masses have considerable **k**-directional dependence. The mass of the Γ_9^6 band is heavy along any **k** direction. On the other hand, that of the Γ_7^6 band is light in the k_x-k_y plane but heavy along k_z direction, and that of the Γ_7^1 band is the very reverse. Further, the Γ_7^1 band is split off from Γ_9^6 and Γ_7^6 bands even without spin-orbit coupling. These features show that the **k**-directional dependence of hole masses is not negligible if we carry out the material design and/or the characteristic analysis of quantum-well devices like LD's. Thus the **k**·**p** perturbation parameters A_i in the WR structure, which correspond to the Luttinger parameters γ_i in the ZB structure, are very significant and useful for technological applications.

According to the experimental result for GaN, the hole mass is $0.8(\pm 0.2)m_0$.[23] On the other hand, the calculated mass of the Γ_9^6 band, which is the lowest in hole energy among the three bands, is quite a bit more heavy than the observed one. However, both the crystal-field and spin-orbit splittings are so small that we estimated the typical hole mass by averaging the **k**-direction-dependent masses with the weight of **k**'s star. Here we considered two (heavy and light) and three (heavy, light, and split-off) bands in averaging hole masses. In both cases, the average hole mass is about $0.95m_0-1.10m_0$, which is consistent with the observed one. This value for the WR-type GaN is much larger than for the conventional ZB materials like GaAs. Such a heavy mass would cause the high carrier density to realize the population inversion. Therefore, a higher carrier density might be neces-

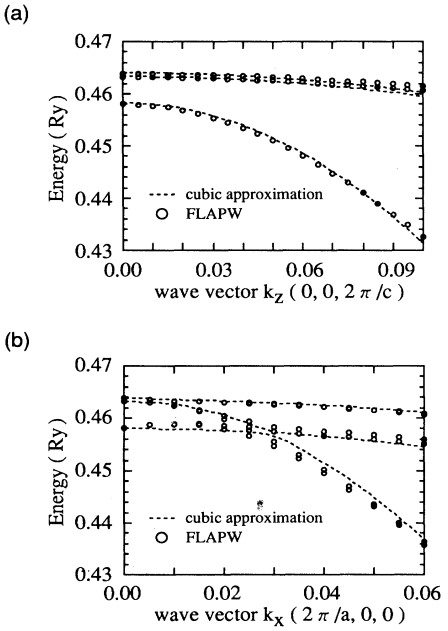

FIG. 4. The finer band structures near the Γ point along (a) k_z and (b) k_x directions with spin-orbit interaction. The results obtained by the FLAPW band calculation (open circles) and the effective-mass theory within the cubic approximation (broken lines) are shown together for comparison.

TABLE III. The hole effective masses for AlN and GaN. $m_{\rm hh}$, $m_{\rm lh}$, and $m_{\rm split}$ denote the heavy-, light-, and split-off-hole masses, and the superscripts $\parallel$ and $\perp$ represent the **k**-directional dependence along the k_z and k_x directions, respectively. All values are in units of a free-electron mass m_0. The results of the line fitting are also listed in round brackets, compared with that of the 3D fitting within the cubic approximation.

	$m_{\rm hh}^{\parallel}$	$m_{\rm lh}^{\parallel}$	$m_{\rm split}^{\parallel}$	$m_{\rm hh}^{\perp}$	$m_{\rm lh}^{\perp}$	$m_{\rm split}^{\perp}$
AlN	3.68	3.68	0.25	6.33	0.25	3.68
	(3.53)	(3.53)	(0.25)	(10.42)	(0.24)	(3.81)
GaN	1.10	1.10	0.15	1.65	0.15	1.10
	(1.76)	(1.76)	(0.16)	(1.61)	(0.14)	(1.04)

sary to obtain sufficient optical gain, if LD's using the WR-type GaN-based materials are fabricated.

As for the energy splittings, the calculated spin-orbit splitting Δ_{so} is in good agreement with the experimental value $0.82(+0.37,-0.15)$ mRy.[25] On the other hand, the calculated crystal-field splitting Δ_{cr} is in disagreement with the experimental value, $1.62(\pm 0.15)$ mRy,[25] though the sign and the relative size to Δ_{so} is in agreement. However, the electronic structures around the VBM are very sensitive to strains. So for more detailed comparison, more accurate measurements using homogeneous strain-free crystals are desirous, and we must perform first-principles calculations with lattice parameters free.

B. Accuracy of cubic approximation

We study the accuracy of the 3D fitting within the cubic approximation, using analytical solutions of the effective-mass Hamiltonian and energy eigenvalues near the Γ point by first-principles calculations. First, we explain the result for the energy splittings. The crystal-field splittings Δ_1 can be determined directly from the difference between Γ_6 and Γ_1 levels by the FLAPW calculation without the spin-orbit interaction. Then, using the obtained Δ_1, the spin-orbit splittings Δ_2 and Δ_3 can be derived from Γ_9, Γ_7, and Γ_7 levels by the FLAPW calculation with the spin-orbit interaction. We call this procedure the Γ-point fitting. The results of the Γ-point fitting are shown in Table II, compared with those of the 3D fitting within the cubic approximation. According to Table II, two kinds of results are nearly equal, and the relation $\Delta_2=\Delta_3$ seems to be good. Therefore, the cubic approximation is fairly suitable for the energy-splitting parameters.

Next, we describe the result of the Luttinger-like parameters. According to first-principles calculations, spin-orbit effects are very small in these nitrides. Thus, for both the analytical expression and the FLAPW calculation, we used results without the spin-orbit interaction. Further, we neglected the contribution of the parameter A_7. Estimating from the energy splitting between E_2 and E_3 in the k_x-k_y plane, A_7 is at most about 10^{-10} Ry cm for GaN. Then, as for the value of $m_{\mathrm{lh}}^{\perp}$, the contribution of $A_7(2A_7^2/|\Delta_1|)$ is about 10^{-2} times as small as those of the other terms $[(A_2+A_4+A_5)]$. Therefore, assuming that $A_7=0$, we obtained A_i $(i=1-5)$ from parabolic fits of the energy dispersions along Δ (for A_1 and A_3) and Σ (for A_2, A_4, and A_5) lines (see Fig. 1), respectively. We call this procedure the line fitting. In Tables II and III, the results of the line fitting are shown with those of the 3D fitting within the cubic approximation. From a comparison between two kinds of results for A_i, the difference between them is less than about 5%. Therefore, the cubic approximation is fairly successful in the analysis of the valence-band structures of WR-type AlN and GaN.

Furthermore, the similarity between WR and ZB structures has been investigated in previous works,[12] where it was reported that the total-energy differences are only ~ 0.01 eV/atom, and that the trends in the band-gap differences can be explained by the band folding and crystal symmetry. From these results as well as our results, it is obvious that the cubic approximation for the WR structure is valid in these nitrides.

V. CONCLUSIONS

In conclusion, we have performed first-principles FLAPW band calculations within the LDA for WR-type AlN and GaN. The electronic properties have been investigated on the basis of the effective-mass approximation, where we consider the hexagonal symmetry of the WR structure. Electron effective mass, hole effective masses, or equivalently, the Luttinger-like parameters, crystal-field splitting and spin-orbit splitting have been derived from reproducing the calculated band structures near the VBM and CBM. The obtained parameters for GaN are almost consistent with the experimental results. All the parameters we presented here will be very useful for a characteristic analysis of quantum-well devices like LD's. We suggest that the cubic approximation is available to analyze the electronic properties of WR-type crystals. Lastly, in order to obtain a more quantitative understanding of the effective-mass parameters, we may need to perform calculations relaxing the values of the lattice parameters a and c and the internal parameter u.

ACKNOWLEDGMENTS

Two of us (M.S. and T.U.) are grateful to S. Kamiyama for his helpful discussions about the characteristics of the device, and to Dr. H. Ogawa for his continual encouragement throughout this study.

[1]R. B. Zetterstrom, J. Mater. Sci. **5**, 1102 (1970).
[2]H. P. Maruska and J. J. Tietjen, Appl. Phys. Lett. **15**, 327 (1969).
[3]W. M. Yim, E. J. Stofko, P. J. Zanzucchi, J. I. Pankove, M. Ettenberg, and S. L. Gilbert, J. Appl. Phys. **44**, 292 (1973).
[4]H. Amano, N. Sawai, I. Akasaki, and Y. Toyoda, Appl. Phys. Lett. **48**, 353 (1986).
[5]S. Nakamura, Jpn. J. Appl. Phys. **30**, L1705 (1991).
[6]H. Amano, M. Kito, K. Hiramatsu, and I. Akasaki, Jpn. J. Appl. Phys. **28**, L2112 (1989).
[7]S. Nakamura, T. Mukai, M. Senoh, and N. Iwasa, Jpn. J. Appl. Phys. **31**, L139 (1992).
[8]W. Y. Ching and B. N. Harmon, Phys. Rev. B **34**, 5305 (1986).
[9]W. R. L. Lambrecht and B. Segal, Phys. Rev. B **43**, 7070 (1991).
[10]P. E. Van Camp, V. E. Van Doren, and J. T. Devreese, Phys. Rev. B **44**, 9056 (1991); Solid State Commun. **81**, 23 (1992).
[11]B. J. Min, C. T. Chan, and K. M. Ho, Phys. Rev. B **45**, 1159 (1992).
[12]C. Yeh, Z. W. Lu, S. Froyen, and A. Zunger, Phys. Rev. B **46**,

10 086 (1992); C. Yeh, S. Wei, and A. Zunger, *ibid.* **50**, 2715 (1994).
[13]L. Wenchang, Z. Kaiming, and X. Xide, J. Phys. Condens. Matter **5**, 875 (1993).
[14]A. Rubio, J. L. Corkill, M. L. Cohen, E. L. Shirley, and S. G. Louie, Phys. Rev. B **48**, 11 810 (1993); A. Rubio, J. L. Corkill, and M. L. Cohen, *ibid.* **49**, 1952 (1994); A. Rubio and M. L. Cohen, *ibid.* **51**, 4343 (1995).
[15]M. Palummo, L. Reining, R. W. Godby, C. M. Bertoni, and N. Bornsen, Europhys. Lett. **26**, 607 (1994).
[16]E. Wimmer, H. Krakauer, M. Weinert, and A. J. Freeman, Phys. Rev. B **24**, 864 (1981).
[17]O. Gunnarson and B. I. Lundquvist, Phys. Rev. B **13**, 4274 (1976).
[18]L. Hedin, Phys. Rev. **139**, A796 (1965).
[19]M. S. Hybertsen and S. G. Louie, Phys. Rev. Lett. **55**, 1418 (1985).
[20]R. W. Godby, M. Schluter, and L. J. Sham, Phys. Rev. Lett. **56**, 2415 (1986).
[21]J. M. Luttinger and W. Kohn, Phys. Rev. **97**, 869 (1955).
[22]G. L. Bir and G. E. Pikus, *Symmetry and Strain-Induced Effects in Semiconductors* (Wiley, New York, 1972), p. 329.
[23]J. I. Pankove, S. Bloom, and G. Harbeke, RCA Rev. **36**, 163 (1975).
[24]A. S. Barker and M. Ilegems, Phys. Rev. B **7**, 743 (1973).
[25]R. Dingle and M. Ilegems, Solid State Commun. **9**, 175 (1971).